Propyne Pyrolysis in a Flow Reactor: An Experimental, RRKM, and Detailed Kinetic Modeling Study

Scott G. Davis*,† and Chung K. Law

Department of Mechanical and Aerospace Engineering, Princeton University, Princeton, New Jersey 08544-5263

Hai Wang*

Department of Mechanical Engineering, University of Delaware, Newark, Delaware 19716-3140

Received: June 24, 1998; In Final Form: May 7, 1999

The pressure-dependent rate coefficients for several reactions relevant to propyne pyrolysis were determined with ab initio quantum mechanical calculations and Rice−Ramsperger−Kassel−Marcus (RRKM) analyses. These reactions include the mutual isomerization of propyne and allene, the chemically activated reactions of propyne and allene with the H atom and of acetylene with methyl on the C_3H_5 potential energy surface. Propyne pyrolysis was experimentally studied in a flow reactor at 1210 K and 1 atm. A detailed reaction mechanism, employing the current RRKM rate coefficients, is shown to accurately predict the experimental acetylene and methane profiles determined in the flow reactor and literature shock-tube data of propyne and allene pyrolysis up to 1500 K.

I. Introduction

The high-temperature pyrolysis of propyne (pC_3H_4) has been extensively studied over the last 2 decades.[1−8] The mechanistic understanding is that propyne initially undergoes a fast isomerization to allene (aC_3H_4) coupled with slower decomposition reactions initiated by CH fission.[2] Levush et al.[1] examined the pyrolysis of allene and propyne at atmospheric pressure and over the temperature range 900−1150 °C. They concluded that the mutual isomerization is faster than CH fission. Lifshitz, Frenklach, and Burcat[2] observed propyne and allene pyrolysis in a single-pulse shock tube over 1040−1470 K and 1.2−6 atm. They detected allene, propyne, methane, acetylene, ethylene, ethane, and H_2 as products of propyne and allene pyrolysis and found that the production of CH_4 is considerably faster from propyne pyrolysis than from allene. Subsequent studies by Hidaka and co-workers[4,5] and by Wu and Kern[6] further confirmed the notion of fast mutual isomerization and the chain mechanism initiated by CH fission. It was further found from these studies that benzene is produced in significant concentrations.

A recent study by Kiefer, Kern, and co-workers[8] used two complementary shock-tube techniques, laser schlieren (LS) and time-of-flight (TOF) mass spectrometry, to examine the thermal decomposition of allene and propyne. The LS experiments over the 1800−2500 K temperature range and 70−650 Torr pressure range show that the dissociation of propyne and allene follows a very weak chain reaction initiated by CH fission, although a small amount of H_2 elimination from allene may be possible. Because the LS technique is capable of eliminating the influences of secondary reactions, the CH fission rates were accurately determined in that study. The TOF experiments over the 1690−2090 K and 240−330 Torr range detect acetylene, methane, diacetylene, and benzene. An important finding of ref 8 was that the rate of the CH fission reactions of propyne and allene observed in the high-temperature and low-pressure LS experiments cannot be explained without considering the hindered rotation in propyne and allene.

From these studies, it has been known that there is a rapid isomerization between propyne and allene and the pyrolysis of these compounds produces mainly acetylene and methane via the chemically activated reactions of the H-atom with propyne and allene, e.g.,

$$pC_3H_4 + H \rightarrow C_2H_2 + CH_3$$

The above reaction belongs to a class of chemically activated reactions on the C_3H_5 potential energy surface. Previously, there are only two high-temperature experimental measurements for the rate coefficient of the above reaction, the first being the forward rate from propyne pyrolysis[5] and the second being the reverse from methane pyrolysis.[9] In both studies, the reaction is of secondary importance in the overall process, as such the reported rate coefficient of the $pC_3H_4 + H$ reaction remains uncertain.

Although an accurate knowledge of the rate coefficient of the $pC_3H_4 + H$ reaction is not critical in order to explain the pyrolysis experiments, this knowledge is critically required for the prediction of the ignition delay times of propyne in a shock tube, and propyne and allene oxidation in general.[10,11] In particular, in fuel-rich flames with abundant H atoms, the reaction of H with pC_3H_4 not only consumes the H atoms and thereby reduces the overall oxidation rate, it also provides an additional route of propyne and allene mutual isomerization via the H-atom catalyzed reaction[8]

$$pC_3H_4 + H \rightarrow aC_3H_4 + H$$

Using the QRRK methodology, Dean and Westmoreland[12] examined the chemically activated process of

$$C_2H_2 + CH_3 \rightarrow \text{products}$$

* Corresponding authors.

† Present address: IRPHE-Laboratoire de Combustion, Service 252, Faculté de St. Jérôme, 13397 Marseille Cedex 20, France.

10.1021/jp982762a CCC: $18.00
Published on Web 07/14/1999

In that study, they demonstrated the importance of chemically activated reactions and the effect of pressure on these reactions. The same reaction system was recently reexamined by Diau, Lin, and Melius,[13] who computed the BAC-MP4 potential energy barriers and determined the pressure-dependent rate coefficients using the RRKM method. In both studies, the isomerization of the energized adducts to form CH_3CCH_2 and its subsequent isomerization/dissociation paths were omitted because it is unlikely that these paths should influence the $C_2H_2 + CH_3$ rates. However, with this omission, the H-atom catalyzed propyne and allene mutual isomerization was also excluded in their studies.

It is known from propyne and allene pyrolysis studies that a significant amount of benzene is produced.[5,6,8] The production of benzene can be attributed to the recombination of propargyl (C_3H_3) radicals.[6,14−17] However, there still exist large uncertainties concerning the self-reaction of propargyl. It is still not known to what extent fulvene, benzene, or phenyl form from a single-step elementary reaction of C_3H_3 recombination.[18,19] These uncertainties affect the understanding of propyne pyrolysis in several ways. First, fulvene/benzene/phenyl formed from propargyl recombination undergo subsequent reactions, leading to molecular mass growth and ultimately soot formation, or they may decompose to small species, like acetylene and diacetylene.[8] Second, if the $C_3H_3 + C_3H_3$ reaction leads to phenyl + H, the H atom would subsequently promote chain reaction via the chemically activated reaction of $pC_3H_4 + H$. The last problem poses a significant challenge in achieving reliable measurements for the $pC_3H_4 + H$ reaction from propyne pyrolysis. For this reason, a further theoretical study is critically needed, and such a study must take into consideration a more complete set of reactions occurring on the C_3H_5 potential energy surface.

In this work, we performed (a) density functional theory (DFT)[20] and G2[21] calculations for the potential energy (PE) barriers and (b) Rice−Ramsperger−Kassel−Marcus (RRKM)[22,23] calculations for the mutual isomerization of propyne and allene, and the chemically activated $pC_3H_4 + H$, $aC_3H_4 + H$, and $C_2H_2 + CH_3$ addition/dissociation reactions. The present analysis includes a more complete description of the potential energy surface of C_3H_5, including allyl (aC_3H_5), CH_3CHCH, CH_3CCH_2, and their dissociation products $C_2H_2 + CH_3$, $pC_3H_4 + H$, and $aC_3H_4 + H$. To examine the accuracy of these results, we compared the theoretical rate coefficients with those available in the literature at both low and high temperatures. We also performed an experimental propyne pyrolysis study in an atmospheric flow reactor at 1210 K to help to evaluate the adequacy of our theoretical results at this moderately high temperature. Using detailed kinetic modeling, we demonstrated that the current theoretical rate coefficients can accurately predict the production of C_2H_2 and CH_4 in the flow reactor experiments and in the shock-tube pyrolysis study of propyne and allene.[5]

In addition to the chemically activated reactions occurring on the C_3H_5 potential energy surface, the mutual isomerization of propyne and allene was also examined in the present study. There have been several theoretical studies[24−28] reported regarding the minimum energy route for the mutual isomerization of propyne and allene. Honjou et al.[24] found that a direct 1,3-H shift requires an excessive energy barrier of about 90 kcal/mol. They proposed that the mutual isomerization of propyne and allene proceeds through the intermediate cyclopropene (cC_3H_4) and more specifically, via

$$pC_3H_4 \rightarrow \text{propenylidene} \rightarrow cC_3H_4 \rightarrow \text{vinylmethylene} \rightarrow aC_3H_4$$

all of which are accessible to internal energy in excess of 65 kcal/mol. Subsequent studies[25−28] further confirmed their findings. Recognizing that cyclopropene may have to be considered as a stabilized intermediate under certain combustion conditions, we also report the pressure-dependent, RRKM rate coefficients determined for the mutual isomerization of propyne and allene. The RRKM parameters were obtained in a similar fashion as those of the C_3H_5 reactions.

II. Methodologies

Experimental. The Princeton turbulent flow reactor (PTFR) used in this work has been extensively documented in previous studies.[29,30] The pyrolysis experiment was performed in the PTFR at atmospheric pressure using propyne with a purity of 98.1%. The major impurities in the gas sample were propane (<0.2%), butane (<0.5%), allene (<0.3), and butenes (<0.7%). The PTFR was operated near its upper design temperature to ensure sufficient reaction progression over the allowable reaction time. Specifically, experiments were conducted at 1210 K with 0.297% propyne in nitrogen. Background levels of oxygen were detected, but never exceeded 160 ppm. It is estimated that these background levels of oxygen never exceeded 60 ppm in the reaction zone of the reactor and that the remaining oxygen contamination occurred in the carrier lines to the sample valves, where the mixture was already quenched. These small levels of oxygen have a minimal effect on the pyrolysis experiment for the present fuel, as confirmed by a subsequent analysis in which a small amount of oxygen (300 ppm) was artificially added to the same initial mixture and the results showed no appreciable changes in the fuel decay and major intermediate species profiles.

Gas samples were collected in a water-cooled sampling probe and analyzed using a 5890 Hewlett-Packard gas chromatograph with FID detectors. C_1 through C_4 hydrocarbon species were eluted from a PlotQ column, while C_5 and higher hydrocarbons were eluted from a DB-5 column. FID signals of the product yields were quantified and converted into mole fractions using extensive calibrations from a gravimetrically blended, certified gas mixture. Carbon balances were carefully checked for each sample and were found to be close to the total initial carbon, and were within ±5% of the mean value. There is no evidence of carbon formation or carbon deposits over the entire course of reaction. GC analysis detected methane, acetylene, ethylene, ethane, propene, allene 1,3-butadiene (1,3-C_4H_6), 1,2-butadiene, vinylacetylene, 2-butyne, butenes, cyclopentadiene, benzene, and toluene.

Ab Initio and RRKM Calculations. Ab initio calculations were carried out using the Gaussian94[31] program. Energy calculations were performed on geometries and frequencies optimized using the hybrid B3LYP density functional, which employs a slightly modified[32] Becke's three-parameter exchange functional (B3)[33] coupled with the correlational functional of Lee, Yang, and Parr (LYP),[34] with the split-valence plus polarization 6-31G(d) basis set. The hybrid B3LYP functional was chosen for its ability to predict reasonably well the geometries for transition states[35] and for free radicals when the spin contamination $\langle S^2 \rangle$ is moderate.[36] The zero-point vibrational energies (ZPVE) were calculated from the harmonic frequencies, which were scaled by a factor of 0.98. This scaling factor was specifically determined for ZPVEs calculated at the B3LYP/6-31G(d) level.[37] A full G2[21] calculation was performed on the B3LYP/6-31G(d) geometries and frequencies, resulting in energies which approximate a QCISD(T)/6-311+G(3df,2p)//B3LYP/6-31G(d) calculation, which will be referred to as G2-

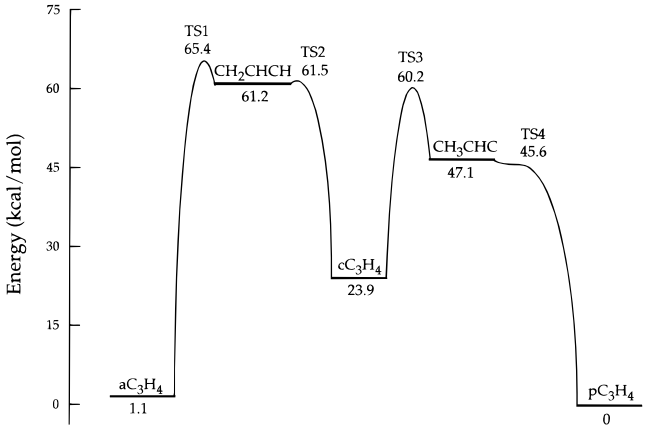

Figure 1. Potential energy barriers of allene and propyne mutual isomerization, determined at the G2(B3LYP) level of theory. For TS1 and TS3, the energies are reduced by 2 and 1 kcal/mol, respectively, from those predicted at G2(B3LYP) level; see text.

(B3LYP). The use of the empirical higher level correction (HLC) was avoided in the present calculations by using relative energies where the HLC cancels exactly. For the C_3H_5 free-radical system spin contamination is low $\langle S^2 \rangle < 0.8$ for all isomers and transition states at the B3LYP/6-31G(d) level.

We employed the analytic gradient procedure and the combined synchronous transit and quasi-Newton (STQN) method for the determination of isomerization transition states.[38] For dissociation reactions, the transition state was determined by a relaxed scan of the potential energy surface. All transition state structures were confirmed by having only one imaginary frequency with the motion along the reaction coordinate.

The frequencies and rotational constants required for RRKM calculations were obtained at the B3LYP/6-31G(d) level and whenever possible at the B3-PW91/6-311G(d,p) level.[39] Both the B3LYP and the B3-PW91 were shown to have the lowest overall root-mean-square error between the theoretical harmonic frequencies (after scaling) and experimental fundamental frequencies.[37] Durant,[35] however, showed that the B3-PW91 functional appears to be better than the B3LYP functional at predicting frequencies for transition state structures. For the C_3H_5 system, theoretical frequencies were calculated at the B3-PW91/6-311G(d,p) level and were scaled by 0.973, as determined by methods described in ref 37. There was, however, little difference (after scaling) between these frequencies and those calculated at the B3LYP/6-31G(d) level for all structures. For the propyne/allene isomerization system, frequencies obtained at the B3LYP/6-31G(d) level had to be used due to convergence problems encountered for transition states using the B3-PW91 functional. Based on the C_3H_5 system, the results should be very comparable. The frequencies obtained at the B3LYP/6-31G(d) level were scaled by 0.96, as recommended by Scott and Radom[37] for the scaling of harmonic frequencies calculated at this level of theory.

Thermal rate coefficients were calculated from the microcanonical rate constants obtained from the RRKM theory,[22,23]

$$k(E) = l_a \frac{Q_r^{\ddagger} W(E^{\ddagger})}{Q_r h \rho(E)'} \qquad (1)$$

where l_a is the reaction degeneracy, $Q_r^{\ddagger}$ and Q_r are respectively the partition functions for inactive rotational degrees of freedom of the transition state and the reactant molecule, $W(E^{\ddagger})$ is the sum of rovibrational energy states of the transition state at energy level $E^{\ddagger}$, $\rho(E)$ is the density of states of the stable species at energy level $E = E^{\ddagger} + E_o$, E_o is the energy barrier, and h is the Planck constant. The direct-count algorithm of Beyer and Swinehart[40] was used to calculate the sums of energy states, while the densities of states were calculated using the Whitten−Rabinovitch approximation.[41] Active rotations were accommodated using the method of Astholz et al.[42] Further details about the RRKM code can be found in ref 43.

The thermal rate coefficients were obtained by assuming a steady state for each of the energized species and by implementing weak collision stabilization. For the propyne/allene isomerization system, the form of the reaction is

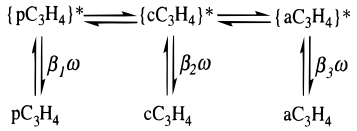

and for the C_3H_5 system, the form of the reaction is

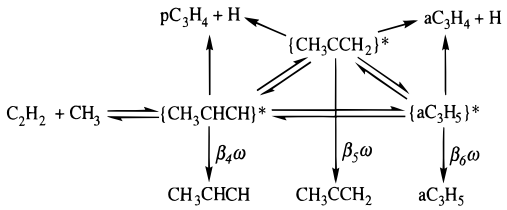

where {}* denotes an excited species and β its corresponding efficiency of collisional stabilization and ω is the collisional frequency. The β's were calculated using the approximation of Gilbert et al.,[44]

$$\beta = \frac{\left(\frac{\langle E_{down} \rangle}{\langle E_{down} \rangle + F_E k_B T}\right)^2}{\int_0^{E_o} B(E)\left[1 - \frac{F_E k_B T}{\langle E_{down} \rangle + F_E k_B T} \exp\left(-\frac{E_o - E}{F_E k_B T}\right)\right] dE} \qquad (2)$$

where $\langle E_{down} \rangle$ is the average energy transferred per collision in down transitions, k_B is the Boltzmann constant, T is the temperature, $B(E)$ is the Boltzmann distribution of energy E, and F_E is the energy-dependent density of states. Because the collision stabilization efficiency depends on the nature of the molecule, β must be different for different excited species. For this reason β_i was computed for each adduct. This was accomplished by assuming E_o in eq 2 to be equal to the minimum energy barrier for the ground-state adduct to dissociate or isomerize. For example, β_4 was computed using the molecular properties of CH_3CHCH (for $B(E)$ and F_E) and with E_o equal to that of the dissociation of CH_3CHCH to $C_2H_2 + CH_3$.

Kinetic Modeling. The modeling of the flow reactor and shock-tube experiments was performed using the Sandia Chemkin II[45] and the Senkin code.[46] A detailed kinetic model was used for the simulation, which was similar to the one used in a previous study of propyne oxidation in a flow reactor and in laminar premixed flames.[11] The kinetic mechanism and its associated thermochemical data will be described later.

III. Mutual Isomerization of Propyne and Allene

The potential energy barriers for the isomerization of propyne and allene are presented in Figure 1. Of critical importance to the rate coefficient calculation are the energies of TS1 and TS3. The present G2(B3LYP) energy barriers of these two transition-state structures agree with those obtained by Yoshimine et al.[26] at the MRCI(DZP) level of theory to within 1.5 kcal/mol. The

TABLE 1: RRKM Parameters of the Allene and Propyne Isomerization Reaction Calculated at the B3LYP/6-31G(d) Level, with All Frequencies Scaled by 0.96 (See Text)

aC_3H_4	υ, cm^{-1}	371, 371, 830, 830, 853, 995, 995, 1078, 1397, 1450, 1992, 3019, 3023, 3088, 3088
	B_0,[a] cm^{-1}	0.296 (4,2) external inactive; 4.863 (1,1) external active
	L−J params[b]	$\sigma = 4.76$ Å; $\epsilon/k_B = 252$ K
pC_3H_4	υ, cm^{-1}	333, 333, 576, 577, 913, 1032, 1032, 1387, 1448, 1448, 2158, 2921, 2981, 2981, 3357
	B_0,[a] cm^{-1}	0.284 (3,2) external inactive; 5.334 (1,1) external active
cC_3H_4	υ, cm^{-1}	578, 766, 826, 899, 982, 1002, 1041, 1082, 1130, 1491, 1683, 2929, 2984, 3138, 3182
	B_0,[a] cm^{-1}	0.580 (2,2) external inactive; 1.005 (1,1) external active
TS1	υ, cm^{-1}	249i, 394, 591, 742, 814, 824, 955, 991, 1153, 1429, 1693, 2605, 2858, 3063, 3147
	B_0,[a] cm^{-1}	0.307 (1,2) external inactive; 3.317 (1,1) external active
TS3	υ, cm^{-1}	926i, 634, 702, 855, 965, 1026, 1040, 1080, 1182, 1443, 1586, 2175, 2967, 3053, 3201
	B_0,[a] cm^{-1}	0.517 (1,2) external inactive; 1.109 (1,1) external active

[a] The numbers in parentheses are the symmetry number and the dimension of the rotor, in that order. [b] Reference 47.

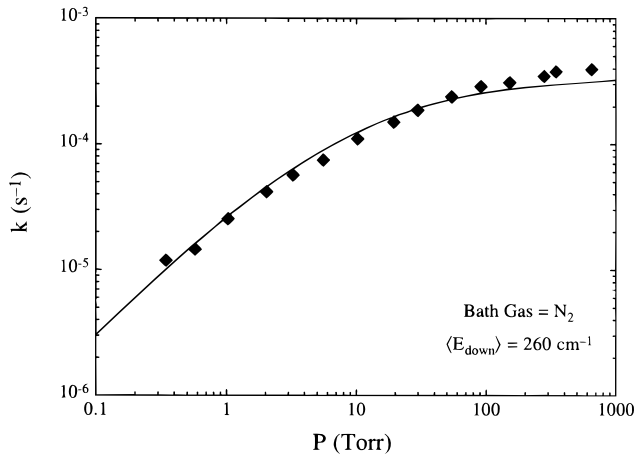

Figure 2. Comparison of the experimental[48] and theoretical rate coefficient of $cC_3H_4 \rightarrow pC_3H_4$ (M = N_2) at 495 K as a function of pressure.

energies of vinylmethylene and propenylidene relative to propyne differ, however, quite substantially from those in ref 26, by as much as 5−7 kcal/mol, possibly because of large spin contamination in these biradical species. These differences are inconsequential since the rate-limiting process is to overcome the potential energy barriers of TS1 and TS3.

The RRKM parameters are presented in Table 1. The reaction path degeneracies are taken into account via the symmetry number; thus, they are explicitly specified as equal to unity in all RRKM calculations. Figure 2 presents a comparison of experimental data of Bailey and Walsh,[48] who studied the isomerization of cC_3H_4, and the present theoretical results at 495 K and over the pressure range 0.3−700 Torr. The calculation uses a reasonable $\langle E_{down} \rangle$ value of 260 cm^{-1} for nitrogen as a bath gas. The experimental data were accurately reproduced over the entire pressure range, as seen in Figure 2, by reducing the G2(B3LYP) energy by 1 kcal/mol for TS3. The theoretical result also shows that the isomerization to aC_3H_4 is

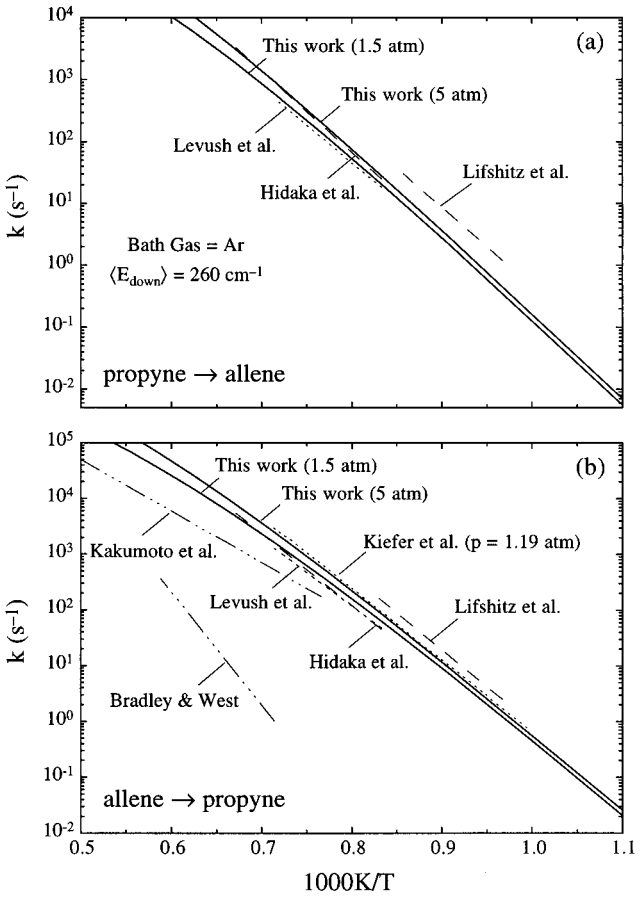

Figure 3. Comparison of the rate coefficients of (a) $pC_3H_4 \rightarrow aC_3H_4$ and (b) $aC_3H_4 \rightarrow pC_3H_4$ at high temperatures between experimental data (Levush et al., 1 atm;[1] Lifshitz et al., 1.19−4.75 atm;[2] Hidaka et al., 1.7−2.6 atm;[5] Bradley and West, 3.95−5.26 atm;[49] Kakumoto et al., [1.13−1.34 × 10^{-5} mol/cm^3][7]) and theoretical results of Kiefer et al.[50] at 1.19 atm and this work (1.5 and 5 atm).

negligible as compared to pC_3H_4 at these conditions, in agreement with the experimental observation.[48]

Figure 3 shows a comparison of the present theoretical results for propyne to allene and allene to propyne at 1.5 and 5 atm with those determined experimentally.[1,2,5,7,49] These two pressures cover the range of pressures employed in the experiments. Comparisons are made by assuming the experimentally measured rate coefficients in each direction are a sum of the direct propyne ↔ allene rate, plus the effective rate due to stabilization to cyclopropene, followed by its re-energization and isomerization to propyne or allene. For example, the total rate for the isomerization from allene to propyne, assuming a steady state for cyclopropene, is given by

$$k_{tot} = k_4 + k_{ss} = k_4 + \frac{k_5 k_6}{k_{-5} + k_6} \tag{3}$$

where the rate coefficients correspond to the reactions given below.

$$aC_3H_4 \rightarrow pC_3H_4 \tag{4}$$

$$aC_3H_4 \leftrightarrow cC_3H_4 \tag{5}$$

$$cC_3H_4 \rightarrow pC_3H_4 \tag{6}$$

For this isomerization process, we found that at 1000 K the direct rate (k_4) is about a factor of 2 larger than the stabilization/redissociation rate (k_{ss}), and it increases to a factor of 15 larger

TABLE 2: RRKM Rate Coefficient Parameters[a] for the Propyne−Allene Isomerization Reaction

		$k = AT^n \exp(-E/RT)$		
	P (atm)	A	n	E
$pC_3H_4 \rightarrow cC_3H_4$	0.1	3.4×10^{46}	−10.97	68.9
	1	1.2×10^{44}	−9.92	69.3
	10	5.3×10^{38}	−8.06	68.3
	100	2.8×10^{31}	−5.69	66.4
	∞	1.7×10^{12}	0.31	60.0
$cC_3H_4 \rightarrow aC_3H_4$	0.1	2.3×10^{39}	−8.81	47.8
	1	4.9×10^{41}	−9.17	49.6
	10	7.2×10^{40}	−8.60	50.6
	100	1.6×10^{35}	−6.64	49.5
	∞	2.0×10^{12}	0.56	42.2
$pC_3H_4 \rightarrow aC_3H_4$[b]	0.1	6.4×10^{61}	−14.59	88.2
	1	5.2×10^{60}	−13.93	91.1
	10	1.9×10^{57}	−12.62	93.3
	100	1.4×10^{52}	−10.86	95.4

[a] Units in s, kcal, mol, and K. Unless otherwise indicated, the rate parameters are fitted within the temperature range 300−2500 K. [b] Fitted for the temperature range 800−2500 K.

at 1500 K. This trend was also observed for the isomerization of propyne to allene. On the basis of this result, it may be necessary to include cyclopropene as an intermediate at low to intermediate temperatures to properly model propyne and allene isomerization.

It is seen in Figure 3 that our theoretical results are in close agreement with the experimental data of Hidaka et al.[5] and Levush et al.,[1] but are lower than the data of Lifshitz et al.[2] by about a factor of 2. Our theoretical results are obtained with the energy of TS1 shifted 2 kcal/mol downward from the original G2(B3LYP) value. Of course, a further decrease in the energy barrier would improve the agreement with the data of Lifshitz et al.[2] The present rate coefficient also differs from the early theoretical results of Kiefer et al.[50] by about a factor of 2. This seems to be consistent with the need of a reduced isomerization rate at high temperatures to avoid an initial gradient not observed in the LS experiments.[8]

Our flow reactor data cannot precisely determine the rate of propyne isomerization to allebe to within a factor 2 of certainty, as will be discussed later. Nonetheless, based on all the experimental and theoretical studies to date, it is tempting to conclude that the uncertainty in our theoretical isomerization rate coefficient is no larger than a factor of 2−3 for temperatures up to 1600 K. For this reason, we tabulate the computed rate coefficients in Table 2 at several representative pressures.

IV. C_3H_5 System

The C_3H_5 system considered here includes the chemically activated reactions of $C_2H_2 + CH_3$, $pC_3H_4 + H$, and $aC_3H_4 + H$, the mutual isomerization, stabilization, and dissociation of the C_3H_5 isomers (aC_3H_5, CH_3CHCH, CH_3CCH_2). The potential energy diagram is presented in Figure 4, and the RRKM parameters are shown in Table 3. The relative energies of propyne, allene, and allyl calculated in the present study support the heat of formation of the allyl radical recently reported by Tsang[51] ($\Delta_f H_{298}$ = 40.9 kcal/mol). Specifically, the present theoretical enthalpies of reaction for $pC_3H_4 + H \rightarrow aC_3H_5$ and $aC_3H_4 + H \rightarrow aC_3H_5$ are −54.9 and −55.9 kcal/mol, respectively, whereas their respective experimental values are −55.5 and −56.8 kcal/mol, based on the well-established $\Delta_f H_{298}$ values of aC_3H_4 (45.6 kcal/mol) and pC_3H_4 (44.3 kcal/mol).[52] The differences are less than 1 kcal/mol, whereas the previous $\Delta_f H_{298}$ = 39.1 kcal/mol[52] yields enthalpies of reaction equal to −57.3 and −58.8 kcal/mol, respectively.

Figure 5 compares the calculated and experimental rate coefficients of the reaction $pC_3H_4 + H \rightarrow$ products at 299, 363, and 460 K. The experimental data were taken from the works of Whytock et al.[53] and Wagner and Zellner.[54] The rate coefficients of Wagner and Zellner[54] were determined over the pressure range of 1−18 Torr with no reported pressure dependence. The theoretical rate coefficients are found to be close, in both magnitude and falloff, to the experimental rates[53] for the three temperatures studied, using an $\langle E_{down} \rangle$ value of 260 cm^{-1} for argon.

Experimental rate coefficients of the reaction $aC_3H_4 + H \rightarrow$ products were compared in Figure 6 with the theoretical results determined in the present study. Aleksandrov et al.[55] studied the reaction in the pressure range 4−4.8 Torr, whereas the data of Wagner and Zellner[56] were obtained between 1 and 20 Torr. RRKM calculations were performed at 4 and 15 Torr with the G2(B3LYP) energy barrier of TS6 increased by 0.5 kcal/mol to reconcile the data reported in the two studies. Wagner and Zellner[56] reported the individual rate coefficients of

$$aC_3H_4 + H \rightarrow CH_3CCH_2 \quad (7)$$

$$\rightarrow aC_3H_5 \quad (8)$$

with k_7 larger than k_8 by about a factor of 6 over the reported temperature range. Our calculation is seen to be in close agreement with the total rate coefficient ($k_7 + k_8$) of ref 56. In addition, the calculated k_7 agrees fairly well with their experimental data. However, the model predicts k_8 to be significantly lower than the experimental value at the low temperature end (300 K), but it is slightly larger than the experimental data at 500 K. Lowering the energy barrier of reaction 8 helps to bring the predicted k_8 to a better agreement with the data of ref 56, but it deteriorates the prediction for the data reported by Tsang and Walker[57] for k_{-8} (allyl dissociation) at 1080 K and 2−7 atm. The current calculations are already larger than their rate by a factor of 3.

Figure 7 compares the experimentally determined data of the recombination reaction $C_2H_2 + CH_3 \rightarrow$ products with the present theoretical results. Holt and Kerr[58] studied this reaction in the pressure range 700−760 Torr, while the results of Garcia-Dominguez and Trotman-Dickenson[59] were obtained between 30 and 90 Torr with their data remodeled by Diau et al.[13] The calculated rates were obtained using a reasonable value of 450 cm^{-1} for $\langle E_{down} \rangle$ at 700 Torr with M = i-C_4H_{10}, and at 60 Torr with M = CH_3CHO. The present theoretical results reproduce quite well these low-temperature data.

In Figure 8, we compare all the major channels of $C_2H_2 + CH_3 \rightarrow$ products, calculated in the present study (solid lines), to those determined in the study of Diau et al.[13] (dashed lines). Also shown is the experimental rate for

$$C_2H_2 + CH_3 \rightarrow pC_3H_4 + H \quad (9)$$

reported by Hidaka et al.[5] for the reverse reaction, in the temperature range 1200−1570 K at pressures between 1.7 and 2.6 atm. The results of Diau et al.[13] were determined at 3 atm, and all of our current calculations were conducted at 2 atm. It is seen that the high-pressure limit and falloff rate coefficients for the $C_2H_2 + CH_3 \rightarrow CH_3CHCH$ reaction agree quite well between the two theoretical studies. One of the largest discrepancies between the two studies is that the present work yields a significant reduction in the rate coefficient of

$$C_2H_2 + CH_3 \rightarrow aC_3H_5 \quad (10)$$

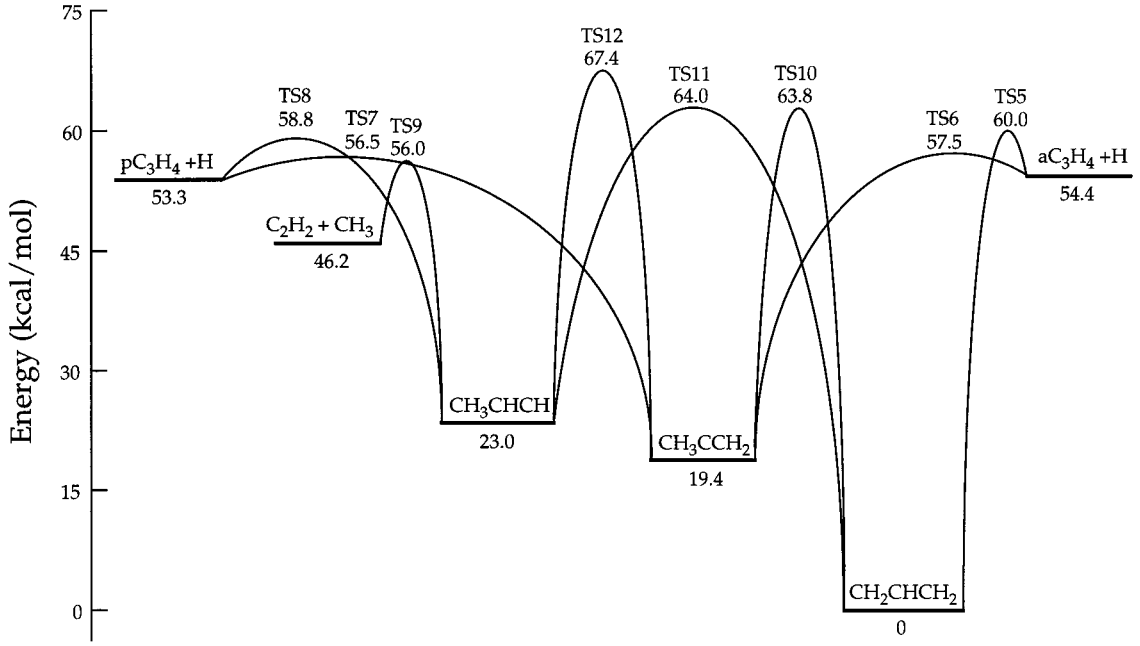

Figure 4. Potential energy barriers of the C_3H_5 system, determined at the G2(B3LYP) level of theory.

TABLE 3: RRKM Parameters of the C_3H_5 System Calculated at the B3-PW91/6-311G(d,p) Level with All Frequencies Scaled by 0.973 (See Text)

aC_3H_5	υ, cm^{-1}	412, 515, 537, 764, 788, 905, 983, 1009, 1177, 1235, 1377, 1469, 1471, 3055, 3059, 3065, 3158, 3161
	B_0,[a] cm^{-1}	0.317 (2,2) external inactive; 1.835 (1,1) external active
	L−J params[b]	$\sigma = 4.85$ Å; $\epsilon/k_B = 260$ K
CH_3CCH_2	υ, cm^{-1}	176, 305, 469, 856, 874, 913, 1016, 1068, 1345, 1372, 1410, 1425, 1711, 2899, 2960, 2984, 3009, 3075
	B_0,[a] cm^{-1}	0.280 (1,2) external inactive; 2.520 (1,1) external active
CH_3CHCH	υ, cm^{-1}	189, 395, 597, 773, 798, 911, 1027, 1080, 1233, 1357, 1437, 1437, 1647, 2944, 2951, 3005, 3049, 3164
	B_0,[a] cm^{-1}	0.303 (1,2) external inactive; 1.929 (1,1) external active
TS5	υ, cm^{-1}	722i, 140, 375, 431, 486, 822, 825, 857, 978, 984, 1062, 1375, 1426, 1939, 3047, 3053, 3129, 3141
	B_0,[a] cm^{-1}	0.287 (1,2) external inactive; 2.123 (1,1) external active
TS6	υ, cm^{-1}	425i, 220, 302, 363, 389, 841, 856, 862, 970, 986, 1068, 1370, 1425, 1977, 3039, 3049, 3115, 3128
	B_0,[a] cm^{-1}	0.271 (1,2) external inactive; 2.248 (1,1) external active
TS7	υ, cm^{-1}	503i, 59[c], 225, 338, 401, 641, 733, 930, 1011, 1020, 1364, 1427, 1429, 2125, 2951, 3016, 3025, 3375
	B_0,[a] cm^{-1}	0.264 (1,2) external inactive; 2.355 (1,1) external active
TS8	υ, cm^{-1}	665i, 154, 358, 411, 454, 633, 655, 921, 1012, 1027, 1365, 1429, 1433, 2091, 2961, 3034, 3034, 3380
	B_0,[a] cm^{-1}	0.278 (1,2) external inactive; 2.229 (1,1) external active
TS9	υ, cm^{-1}	448i, 47[c], 231, 436, 471, 530, 632, 724, 744, 804, 1366, 1374, 1873, 3014, 3176, 3187, 3299, 3388
	B_0,[a] cm^{-1}	0.212 (1,2) external inactive; 1.307 (1,1) external active
TS10	υ, cm^{-1}	1864i, 297, 394, 676, 808, 811, 946, 990, 1066, 1109, 1377, 1405, 1645, 2146, 2981, 2995, 3109, 3113
	B_0,[a] cm^{-1}	0.289 (1/2[d],2) external inactive; 2.575 (1,1) external active
TS11	υ, cm^{-1}	2092i, 444, 617, 670, 870, 893, 914, 1019, 1024, 1096, 1194, 1379, 1600, 1806, 2988, 3056, 3083, 3107
	B_0,[a] cm^{-1}	0.381 (1,2) external inactive; 1.286 (1,1) external active
TS12	υ, cm^{-1}	2038i, 148, 240, 352, 590, 805, 883, 1000, 1002, 1341, 1420, 1427, 1816, 2325, 2923, 2975, 3006, 3027
	B_0,[a] cm^{-1}	0.280 (1,2) external inactive; 2.556 (1,1) external active

[a] The numbers in parentheses are the symmetry number and the dimension of the rotor, in that order. [b] Reference 47. [c] The vibrational motion is replaced by an internal free rotor,[23] and the frequency is not used in the RRKM calculation. [d] The symmetry number of 1/2 was implemented to account for the asymmetric transition state structure which accounts for the proper path degeneracy.[22]

at higher temperatures, while the result of Diau et al. shows a persistent increase in k_{10} as temperature increases. The reason for this discrepancy is the inclusion of allyl dissociation to $aC_3H_4 + H$ in the present study, which has a significant influence on the rate coefficients of k_{10}.

The two theoretical studies yield k_9 values which differ by about a factor of 5, with the present result being larger. The experimental rate determined by Hidaka et al.[5] lies between the two theoretical results. As will be demonstrated later, the production rates of acetylene and methane in the shock-tube experiments of Hidaka et al.,[5] from which k_9 was determined, are not very sensitive to this reaction, as such its rate coefficient cannot be precisely determined. It will be further shown that the concentrations of acetylene and methane can be predicted quite well in the propyne and allene pyrolysis experiments of ref 5, when the present theoretical k_9 is employed.

Table 4 presents the rate coefficient expressions of the C_3H_5 system, determined from the RRKM analysis at several representative pressures.

V. Propyne Pyrolysis in Flow Reactor

In Figure 9, we present selected species profiles experimentally determined for propyne pyrolysis in PTFR at 1210 K and 1 atm. We found that the extent of reaction was quite significant at the first sampling point of PTFR. The propyne mole fraction was found to be 2250 ppm, compared to 2970 ppm in the unreacted mixture. This is most certainly caused by propyne-to-allene isomerization reaction in the mixer section of the flow reactor. The allene concentration at the first sampling point reaches as high as 700 ppm, which continues to rise rapidly to 850 ppm within the initial 20−30 ms, followed by a mild decrease over the remainder of the reaction time. Other product

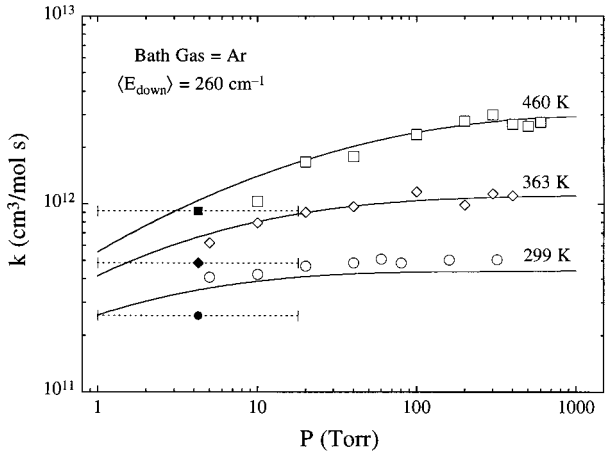

Figure 5. Comparison of the experimental (open symbols, Whytock et al.;[53] solid symbols, Wagner and Zellner[54]) and calculated rate coefficient of $pC_3H_4 + H \rightarrow$ products at 299, 363, 460 K.

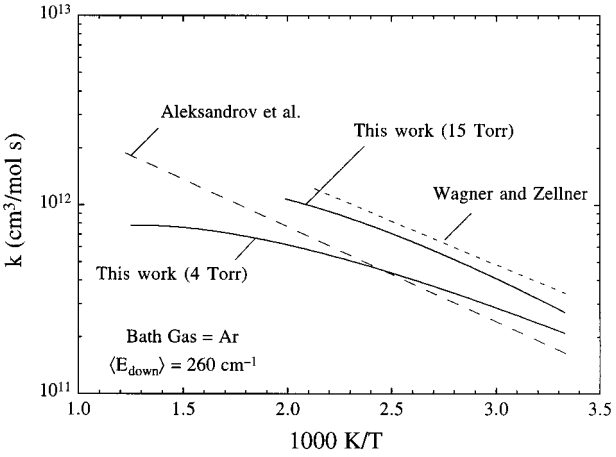

Figure 6. Comparison of the experimental (Aleksandrov et al.,[55] 4−4.8 Torr; Wagner and Zellner,[56] 1−20 Torr) and calculated rate coefficient of $aC_3H_4 + H \rightarrow$ products.

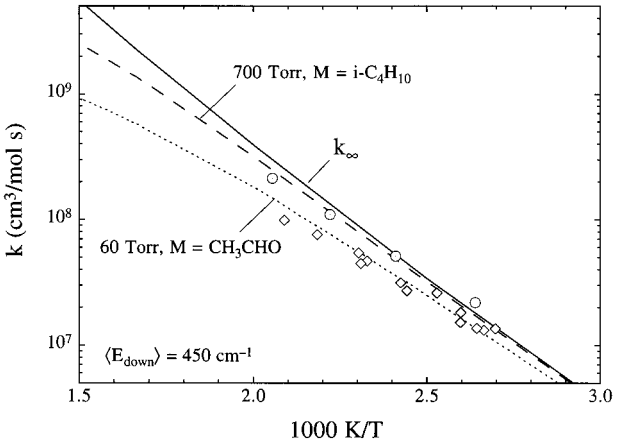

Figure 7. Comparison of the experimental (circles) Holt and Kerr,[58] 700−760 Torr; (diamonds) from Diau et al.[13] who remodeled the data of Garcia-Dominguez and Trotman-Dickenson,[59] 30−90 Torr) and calculated rate coefficient of $C_2H_2 + CH_3 \rightarrow$ products.

species with notable concentrations are acetylene, methane, and benzene, whose mole fractions exceed 100 ppm. 1,3-Butadiene and ethylene were also measured in appreciable concentrations, reaching about 40 ppm at 200 ms. Other species that are detected have concentrations at the ppm level.

It turned out that a satisfactory prediction of the species profiles in the flow reactor was extremely difficult for reasons

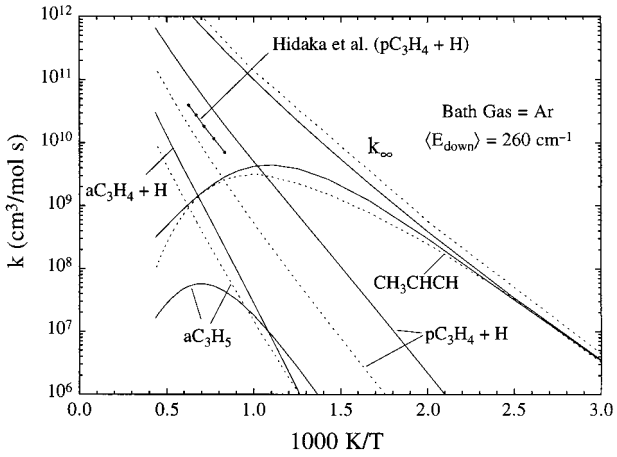

Figure 8. Comparison of the experimental (Hidaka et al.,[5] 1.7−2.6 atm) and theoretical ((dotted lines) Diau et al.,[13] 3 atm; (solid lines) present work, 2 atm) rate coefficients of $C_2H_2 + CH_3 \rightarrow$ products.

which will be discussed later. Nonetheless, we proceeded to compile a reaction mechanism with the aim of verifying the theoretical rate constants described in the previous sections. In this reaction mechanism, the reactions were extracted from the C/H part of a kinetic model previously used for propyne oxidation in a flow reactor and in flames.[11] Several rate parameters were updated based on the theoretical study presently conducted. A set of relevant reactions are presented in Table 5, which essentially yield identical results as the full mechanism for the flow reactor experiments just described and for the shock-tube simulation to be discussed. The thermochemical data for most of the species found in Table 5 were taken from the compilation of Burcat and McBride.[52] The entropy of the propargyl radical was corrected by −7 cal/mol K from the initial compilation.

The essential feature of this mechanism includes the mutual isomerization of propyne and allene, including cyclopropene as a possible intermediate, and the chemically activated reactions of H atoms with propyne and allene, whose rate coefficients were based on the present RRKM study. In an initial attempt to simulate the flow reactor experiments, we found that the fuel decay rate is extremely sensitive to the propyne dissociation rate. In a recent study, Kiefer et al.[8] reported that a standard RRKM−Gorin model significantly underpredicts the rates of propyne and allene dissociation

$$pC_3H_4 \rightarrow C_3H_3 + H \quad (11)$$

$$aC_3H_4 \rightarrow C_3H_3 + H \quad (12)$$

observed in the high-temperature and low-pressure LS experiments. They proposed a hindered-rotor model, which describes the dissociation rates very well. The effects of hindered rotors on unimolecular falloff have been further reviewed by Kiefer.[63]

At the flow reactor conditions of 1210 K and 1 atm, reactions 11 and 12 should be in falloff. Knowledge of the falloff rates is rather limited at this time. The closest rate data that we could take from the literature were those of Kiefer et al.'s RRKM results[8] and those of Hidaka et al.[5] at a pressure of 2.2 atm. The latter experimental data were from rather indirect measurements with possible complications due to H production from propargyl recombination. At 1200 K and 2.2 atm, the second-order dissociation rates of ref 8 are about 1×10^3 cm^3 mol^{-1} s^{-1} for propyne and allene dissociation. The $H + C_3H_3$ combination rate constants k_{-11} and k_{-12} were calculated from these dissociation rates to be 2×10^{13} and 7×10^{12} cm^3 mol^{-1}

TABLE 4: RRKM Rate Coefficient Parameters[a] for the C_3H_5 System

	P	$k = AT^n \exp(-E/RT)$			
	(atm)	A	n	E	note
$C_2H_2 + CH_3 \rightarrow pC_3H_4 + H$	0.1	4.5×10^{06}	1.86	11.6	
	1	2.6×10^{09}	1.10	13.6	
	10	1.1×10^{12}	0.39	16.2	
	100	2.1×10^{12}	0.37	18.1	
$C_2H_2 + CH_3 \rightarrow CH_3CHCH$	0.1	1.4×10^{32}	−7.14	10.0	*b*
	1	3.2×10^{35}	−7.76	13.3	*b*
	10	2.4×10^{38}	−8.21	17.1	*b*
	100	1.4×10^{39}	−8.06	20.2	*b*
	∞	1.5×10^{07}	1.87	8.2	
$C_2H_2 + CH_3 \rightarrow aC_3H_4 + H$	0.1	2.4×10^{09}	0.91	20.7	
	1	5.1×10^{09}	0.86	22.1	
	10	5.1×10^{11}	0.35	25.0	
	100	7.3×10^{12}	0.11	28.5	
$C_2H_2 + CH_3 \rightarrow CH_3CCH_2$	0.1	6.8×10^{20}	−4.16	18.0	*b*
	1	5.0×10^{22}	−4.39	18.8	*b*
	10	9.3×10^{27}	−5.55	22.9	*b*
	100	3.8×10^{36}	−7.58	31.3	*b*
$C_2H_2 + CH_3 \rightarrow aC_3H_5$	0.1	8.2×10^{53}	−13.32	33.2	*b*
	1	2.7×10^{53}	−12.82	35.7	*b*
	10	4.4×10^{49}	−11.40	36.7	*b*
	100	3.8×10^{44}	−9.63	37.6	*b*
$pC_3H_4 + H \rightarrow CH_3CHCH$	0.1	1.0×10^{25}	−5.00	1.8	*b*
	1	5.5×10^{28}	−5.74	4.3	*b*
	10	1.0×10^{34}	−6.88	8.9	*b*
	100	9.7×10^{37}	−7.63	13.8	*b*
	∞	3.2×10^{09}	1.43	4.7	
$pC_3H_4 + H \rightarrow aC_3H_4 + H$	0.1	2.3×10^{15}	−0.26	7.6	
	1	6.3×10^{17}	−0.91	10.1	
	10	3.1×10^{22}	−2.18	14.8	*b*
	100	6.4×10^{27}	−3.58	21.2	*b*
$pC_3H_4 + H \rightarrow CH_3CCH_2$	0.1	4.6×10^{44}	−10.21	10.2	*b*
	1	1.7×10^{47}	−10.58	13.7	*b*
	10	7.0×10^{47}	−10.40	16.6	*b*
	100	3.2×10^{44}	−9.11	17.4	*b*
	∞	1.7×10^{11}	0.97	2.8	
$pC_3H_4 + H \rightarrow aC_3H_5$	0.1	1.1×10^{60}	−14.56	28.1	*b*
	1	4.9×10^{60}	−14.37	31.6	*b*
	10	2.2×10^{59}	−13.61	34.9	*b*
	100	1.6×10^{55}	−12.07	37.5	*b*
$aC_3H_4 + H \rightarrow CH_3CHCH$	0.1	1.1×10^{30}	−6.52	15.2	
	1	5.4×10^{29}	−6.09	16.3	
	10	2.6×10^{31}	−6.23	18.7	
	100	3.2×10^{31}	−5.88	21.5	
$aC_3H_4 + H \rightarrow CH_3CCH_2$	0.1	9.2×10^{38}	−8.65	7.0	*b*
	1	9.5×10^{42}	−9.43	11.2	*b*
	10	1.5×10^{45}	−9.69	15.1	*b*
	100	1.8×10^{43}	−8.78	16.8	*b*
	∞	4.4×10^{09}	1.45	2.4	
$aC_3H_4 + H \rightarrow aC_3H_5$	0.1	9.6×10^{61}	−14.67	26.0	*b*
	1	1.5×10^{59}	−13.54	26.9	*b*
	10	2.4×10^{52}	−11.30	25.4	*b*
	100	6.9×10^{41}	−8.06	21.3	*b*
	∞	4.6×10^{09}	1.44	4.8	
$aC_3H_5 \rightarrow CH_3CHCH$	0.1	1.3×10^{55}	−14.53	73.8	
	1	5.0×10^{51}	−13.02	73.3	
	10	9.7×10^{48}	−11.73	73.7	
	100	1.1×10^{44}	−9.84	73.4	
$aC_3H_5 \rightarrow CH_3CCH_2$	0.1	3.9×10^{59}	−15.42	75.4	
	1	7.1×10^{56}	−14.08	75.9	
	10	6.4×10^{51}	−12.12	75.7	
	100	2.8×10^{43}	−9.27	74.0	
$CH_3CCH_2 \rightarrow CH_3CHCH$	0.1	1.6×10^{44}	−12.16	52.2	
	1	1.5×10^{48}	−12.71	53.9	
	10	5.1×10^{52}	−13.37	57.2	
	100	5.8×10^{51}	−12.43	59.2	

[a] Units in cm, s, mol, kcal, and K. Unless otherwise indicated, the rate parameters are fitted within the temperature range 300−2500 K. [b] Fitted for the temperature range 600−2500 K.

s^{-1} for propyne and allene, respectively. To account for the possible pressure falloff effect, we reduced k_{-11} to 1.5×10^{13} $cm^3\ mol^{-1}\ s^{-1}$ as a rough estimate for simulation under the flow reactor condition of 1210 K and 1 atm. The value of k_{-12} was not very critical to the prediction of the flow reactor experiments. A factor of 2 difference in k_{-12} does not cause any marked changes in the predicted concentration profiles of all species. In the present mechanism, we assigned k_{-12} to be equal to 2.5×10^{12} $cm^3\ mol^{-1}\ s^{-1}$ to represent an average value over 1200−1500 K, a temperature range corresponding to Hidaka et al.'s experiments[5] that were also used in the present model study.

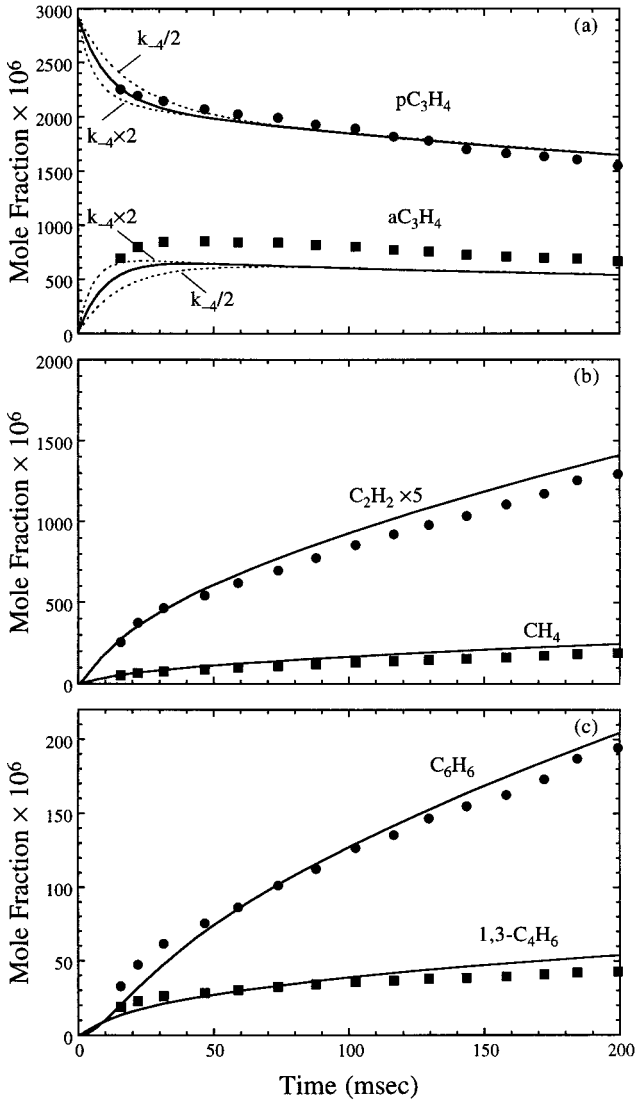

Figure 9. Experimental (symbols) and computed (lines) profiles of selected species in pyrolysis of 0.297% propyne in nitrogen in PTFR at 1 atm, 1210 K. The computation was performed by including 0.7% propane, 0.3% allene, and 0.7% 1-butene as the impurities in the propyne feed. The solid lines represent the base calculation. The dotted lines are obtained with the rate coefficient of $pC_3H_4 = aC_3H_4$ multiplied or divided by 2, as indicated.

It is assumed that the recombination rate of the propargyl radical leading to benzene is 2×10^{12} $cm^3\ mol^{-1}\ s^{-1}$, which was derived from a previous study of benzene formation in a premixed fuel-rich ethylene flame.[18] The second reaction channel leading to the production of phenyl and H atom was also included,

$$C_3H_3 + C_3H_3 \rightarrow C_6H_5 + H \quad (13) \qquad (13)$$

with a rate constant of 5×10^{12} $cm^3\ mol^{-1}\ s^{-1}$. We note that, in terms of predicting the consumption of propyne in the flow reactor, the rate assigned for the above reaction is highly coupled with the propyne and allene dissociation rates. A larger rate of

TABLE 5: Selected Reactions of Propyne Pyrolysis Mechanism[a]

reaction[b]	$k = AT^n \exp(-E/RT)$[c] A	n	E	refs/notes
$pC_3H_4 \rightleftharpoons aC_3H_4$	5.15×10^{60}	−13.93	91117	this work, 1 atm
	7.64×10^{59}	−13.59	91817	2 atm
$pC_3H_4 \rightleftharpoons cC_3H_4$	1.20×10^{44}	−9.92	69250	this work, 1 atm
	5.47×10^{42}	−9.43	69089	2 atm
$cC_3H_4 \rightleftharpoons aC_3H_4$	4.89×10^{41}	−9.17	49594	this work, 1 atm
	8.81×10^{41}	−9.15	50073	2 atm
$C_3H_3 + H \rightleftharpoons pC_3H_4$	1.50×10^{13}			1200 K only, see text
$C_3H_3 + H \rightleftharpoons aC_3H_4$	2.50×10^{12}			1200 K only, see text
$C_2H_2 + CH_3 \rightleftharpoons pC_3H_4 + H$	2.56×10^{09}	1.1	13644	this work, 1 atm
	2.07×10^{10}	0.85	14415	2 atm
$C_2H_2 + CH_3 \rightleftharpoons aC_3H_4 + H$	5.14×10^{09}	0.86	22153	this work, 1 atm
	1.33×10^{10}	0.75	22811	2 atm
$aC_3H_4 + H \rightleftharpoons C_3H_3 + H_2$	1.30×10^{06}	2.0	5500	18
$pC_3H_4 + H \rightleftharpoons C_3H_3 + H_2$	1.30×10^{06}	2.0	5500	18
$aC_3H_4 + CH_3 \rightleftharpoons C_3H_3 + CH_4$	1.30×10^{12}		7700	6, *e*
$pC_3H_4 + CH_3 \rightleftharpoons C_3H_3 + CH_4$	1.80×10^{12}		7700	6, *e*
$pC_3H_4 + H \rightleftharpoons aC_3H_4 + H$	6.27×10^{17}	−0.91	10079	this work, 1atm
	1.50×10^{18}	−1.0	10756	2 atm
$C_3H_3 + C_3H_3 \rightleftharpoons C_6H_6$	2.00×10^{12}			18
$C_3H_3 + C_3H_3 \rightleftharpoons C_6H_5 + H$	5.00×10^{12}			see text
$C_3H_3 + CH_3(+M) \rightleftharpoons 1,2\text{-}C_4H_6(+M)$	1.50×10^{12}			this work, k_∞
	2.60×10^{57}	−11.94	9770	k_0/[M], *d*
$a = 0.175$, $T^{***} = 1341$, $T^* = 60000$, $T^{**} = 9770$				*f*
$CH_3 + H(+M) \rightleftharpoons CH_4(+M)$	1.27×10^{16}	−0.63	383	60, k_∞
	2.48×10^{33}	−4.76	2440	k_0/[M], *d*
$a = 0.783$, $T^{***} = 74$, $T^* = 2941$, $T^{**} = 6964$				*f*
$CH_4 + H \rightleftharpoons CH_3 + H_2$	6.60×10^{08}	1.62	10840	60
$C_2H_2 + H(+M) \rightleftharpoons C_2H_3(+M)$	5.60×10^{12}		2400	60, k_∞
	3.80×10^{40}	−7.27	7220	k_0/[M], *d*
$a = 0.7507$, $T^{***} = 98.5$, $T^* = 1302$, $T^{**} = 4167$				*f*
$C_2H_3 + H(+M) \rightleftharpoons C_2H_4(+M)$	6.08×10^{12}	0.27	280	60, k_∞
	1.40×10^{30}	−3.86	3320	k_0/[M], *d*
$a = 0.782$, $T^{***} = 207.5$, $T^* = 2663$, $T^{**} = 6095$				*f*
$C_2H_3 + H \rightleftharpoons C_2H_2 + H_2$	6.00×10^{13}			60
$C_2H_4(+M) \rightleftharpoons H_2 + C_2H_2(+M)$	8.00×10^{12}	0.44	88770	60, k_∞
	7.00×10^{50}	−9.31	99860	k_0/[M], *d*
$a = 0.7345$, $T^{***} = 180$, $T^* = 1035$, $T^{**} = 5417$				*f*
$C_2H_4 + H \rightleftharpoons C_2H_3 + H_2$	1.33×10^{06}	2.53	12240	60
$C_2H_4 + CH_3 \rightleftharpoons C_2H_3 + CH_4$	2.27×10^{05}	2.0	9200	60
$C_2H_2 + C_2H_3 \rightleftharpoons C_4H_4 + H$	2.00×10^{18}	−1.68	10600	43b, 1 atm
$C_2H_4 + C_2H_3 \rightleftharpoons 1,3\text{-}C_4H_6 + H$	2.80×10^{21}	−2.44	14720	18, 1 atm
$1,3\text{-}C_4H_6 + H \rightleftharpoons pC_3H_4 + CH_3$	7.00×10^{12}		2000	18
$1,2\text{-}C_4H_6 + H \rightleftharpoons 1,3\text{-}C_4H_6 + H$	2.00×10^{13}		4000	18
$1,2\text{-}C_4H_6 + H \rightleftharpoons aC_3H_4 + CH_3$	2.00×10^{13}		2000	18
$1,2\text{-}C_4H_6 + H \rightleftharpoons pC_3H_4 + CH_3$	2.00×10^{13}		2000	18
$1,2\text{-}C_4H_6 \rightleftharpoons 1,3\text{-}C_4H_6$	1.00×10^{13}		65000	18
$c\text{-}C_6H_4 + H \rightleftharpoons C_6H_5$	2.40×10^{60}	−13.66	29500	43b
$C_6H_6 + H \rightleftharpoons C_6H_5 + H_2$	2.50×10^{14}		16000	61
$C_6H_5 + H(+M) \rightleftharpoons C_6H_6(+M)$	1.00×10^{14}			18, k_∞
	6.60×10^{75}	−16.3	7000	k_0/[M]
$a = 1$, $T^{***} = 0.1$, $T^* = 585$, $T^{**} = 6113$				*f*
$C_3H_2 + H \rightleftharpoons C_3H_3$	1.00×10^{13}			estimated
$C_3H_3 + H \rightleftharpoons C_3H_2 + H_2$	5.00×10^{13}		1000	62

[a] Simulation using the reactions included in the table yields results in Figure 9 identical to the full mechanism. [b] Reactions with the sign "⇌" are reversible. [c] Units in cm, s, mol, cal, and K. [d] Third-body enhancement factors: Ar = 0.7. [e] A factor slightly reduced from that originally proposed in ref 6, 2.00×10^{12}. [f] Troe's broadening factor, $F_c(T) = (1 - a) \exp(-T/T^{***}) + a \exp(-T/T^*) + \exp(-T^{**}/T)$.[44]

the above reaction can be compensated by smaller propyne and allene dissociation rates. For these reasons, the rate constants assigned for k_{11}, k_{12}, and k_{13} serve only the purpose of reproducing the propyne disappearance rate in the flow reactor so that we can compare the experimental and predicted acetylene and methane concentrations.

The present kinetic model excludes the contribution of the $pC_3H_4 + C_3H_3$ and $aC_3H_4 + C_3H_3$ reactions to benzene and H-atom production in the flow reactor. The addition/elimination reactions

$$pC_3H_4 + C_3H_3 \rightarrow lC_6H_6 + H$$

$$aC_3H_4 + C_3H_3 \rightarrow lC_6H_6 + H$$

produce "linear" lC_6H_6, which can isomerize to benzene, a proposal originating from Wu and Kern.[6] We note that the endothermicity of the above reactions is greater than 17 kcal/mol if the lC_6H_6 is $CH_2{=}C{=}CH{-}CH{=}C{=}CH_2$ with $\Delta_f H_{298} =$ 92 kcal/mol.[8] Adding ~3 kcal/mol for the activation energy of the $lC_6H_6 + H$ combination reaction, it is expected that the activation energy of addition/elimination reactions is at least 20 kcal/mol. Using this activation energy value and a reasonable *A* factor of 10^{13} cm^3 mol^{-1} s^{-1}, we performed a modeling test and found these reactions to be unimportant to both fuel decay and benzene production rates under the present flow reactor conditions.

There is yet another complication, which arises from the impurity effect in the experiment. This effect was also found to be highly coupled to reaction 13. In the initial tests, we excluded reaction 13 and found that the computed propyne

disappearance rates differ very little with or without the impurities being included in the computation. This is certainly caused by the strong radical-chain inhibition in the system of propyne pyrolysis without the additional source of the H atom due to reaction 13. When reaction 13 was included in the reaction mechanism, however, the overall decomposition rate becomes very sensitive to impurities. In the subsequent computational runs, this impurity effect was included in the computation by assuming that the propyne feed contains 0.7% propane, 0.3% allene, and 0.7% 1-butene.

Figure 9 presents the comparison between the experimental and computed species profiles in the flow reactor, plotted as a function of reaction time. The solid lines represent the base calculation using the mechanism of Table 5. To properly compare the experimental and computed results, the experimental data were time-shifted by +10 ms to account for nonidealities in the mixing process which tend to accelerate initial fuel consumption.[64] It is seen that with a proper prediction of the propyne disappearance rate, the acetylene and methane concentration profiles are predicted well by the model. Unfortunately, this agreement does not provide sufficient support for the current theoretical rate constants. The production rates of acetylene and methane were found to be more sensitive to the CH fission of propyne and allene and to the propargyl recombination reactions. An increase in k_9 by a factor of 2 causes only a 10% increase in the acetylene concentration at 200 ms, while a decrease in k_9 by factors of 2 and 5 reduces the acetylene concentration by 10 and 30%, respectively. The use of k_9 from ref 13 results in the computed acetylene concentrations, which are about 50% lower than the experimental data.

The concentration profiles of 1,3-butadiene and benzene were well reproduced. Based on the current reaction mechanism, 1,3-butadiene is produced primarily from

$$pC_3H_4 + CH_3 \rightarrow 1,3\text{-}C_4H_6 + H$$

Benzene comes almost entirely from propargyl recombination. The current reaction mechanism underpredicts allene concentrations, but the discrepancy between model and experiment is not caused by the uncertainty in the mutual isomerization rate of propyne and allene. An increase or decrease of k_4 by a factor of 2 causes changes in the concentrations of these species only at the very early stage of reaction (see Figure 9a). Thus, a larger rate constant consistent with the experimental measurements of Lifshitz et al.[2] (Figure 3) and the theoretical results of ref 50 could equally describe propyne isomerization to allene in the current PTFR experiment.

VI. Simulation of Propyne and Allene Pyrolysis in Shock Tubes

We performed simulation under the shock-tube condition of Hidaka et al.[5] from 1200 to 1500 K. The mechanism of Table 5 (with rate coefficients at 2 atm) predicts quite well the species distribution as a function of temperature for shock-tube pyrolysis of propyne and allene,[5] as shown in Figures 10 and 11. Although the current rate coefficient for $pC_3H_4 + H \rightarrow C_2H_2 + CH_3$ is a factor of 3 larger than that of Hidaka et al.,[5] the acetylene and methane profiles in these experiments were still well reproduced.

VII. Summary

The pressure-dependent rate parameters of several reaction steps in propyne and allene pyrolysis were examined with ab initio quantum mechanical calculations and RRKM analyses. These reactions include the mutual isomerization of propyne and allene, and the chemically activated reactions of propyne and allene with the H atom and of acetylene with methyl on the C_3H_5 potential energy surfaces. The RRKM rate coefficients were carefully compared with available literature data at both low and high temperatures. The current theoretical results show that the rate coefficient of the reaction

$$C_2H_2 + CH_3 \rightarrow pC_3H_4 + H$$

was a factor of 3 larger than the experimental rate of Hidaka[5] and about a factor of 5 larger than the RRKM rates of Diau et al.[13] It was demonstrated that the production of acetylene and methane from propyne decomposition in the shock-tube experiments of ref 5 can be well accounted for by a detailed reaction mechanism employing the theoretical rates determined in the present study. Propyne pyrolysis was also studied in a flow reactor at 1 atm and 1210 K. Despite many uncertainties, it was shown that the reaction mechanism predicts well the acetylene and methane production rates when the propyne disappearance rate is adequately accounted for.

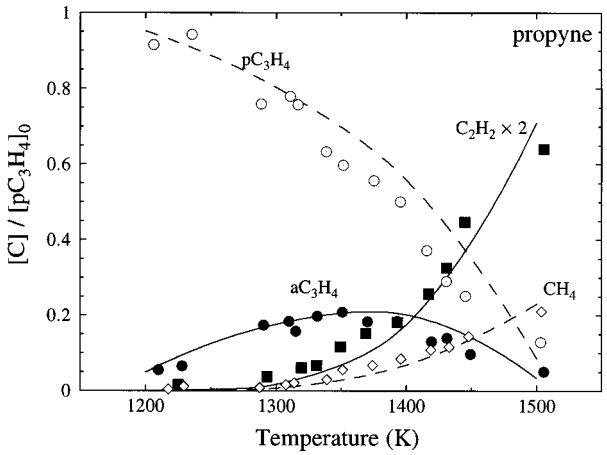

Figure 10. Comparison of experimental[5] (symbols) and computed (lines) species profiles in shock-tube pyrolysis of 4% propyne in argon at 1.7−2.6 atm. The reaction times at 1200, 1300, 1400, and 1500 K are respectively 2400, 2130, 1950, and 1800 μs.

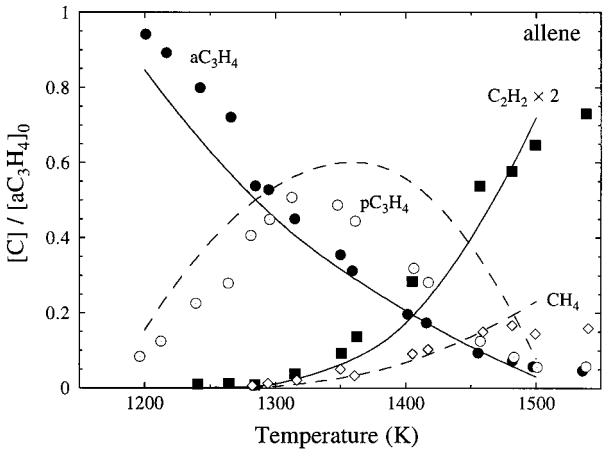

Figure 11. Comparison of experimental[5] (symbols) and computed (lines) species profiles in shock-tube pyrolysis of 4% allene in argon at 1.7−2.6 atm. The reaction times at 1200, 1300, 1400, and 1500 K are respectively 2400, 2130, 1950, and 1800 μs.

Acknowledgment. The authors thank Mr. Joe Sivo for his generous help in the PTFR experiment and Professors Irvin Glassman and Fredrick L. Dryer for making the PTFR facility accessible to us. We also thank Professor John Kiefer of

University of Illinois, Chicago, for many helpful discussions. The work was supported by the New World Vista Program of the Air Force Office of Scientific Research under the technical monitoring of Dr. Julian M. Tishkoff. Quantum mechanical calculations were performed at the Facility for Computational Chemistry at the University of Delaware, which is funded by the NSF (CTS-9724404).

References and Notes

(1) Levush, S. S.; Abadzhev, S. S.; Shevcchuk, V. U. *Neftechim.* **1969**, *9*, 215.
(2) Lifshitz, A.; Frenklach, M.; Burcat, A. *J. Phys. Chem.* **1975**, *79*, 1148.
(3) Lifshitz, A.; Frenklach, M.; Burcat, A. *J. Phys. Chem.* **1976**, *80*, 2437.
(4) Hidaka, Y.; Chimori, T.; Suga, M. *Chem. Phys. Lett*. **1985**, *119*, 435.
(5) Hidaka, Y.; Nakamura, T.; Miyauchi, A.; Shiraishi, T.; Kawano, H. *Int. J. Chem. Kinet.* **1989**, *21*, 643.
(6) Wu, C. H.; Kern, R. D. *J. Phys. Chem.* **1987**, *91*, 6291.
(7) Kakumoto, T.; Ushirogouchi, T.; Saito, K.; Imamura, A. *J. Phys. Chem.* **1987**, *91*, 183.
(8) Kiefer, J. H.; Mudipalli, P. S.; Sidhu, S. S.; Kern, R. D.; Jursic, B. S.; Xie, K.; Chen, H. *J. Phys. Chem. A* **1997**, *101*, 4057.
(9) Hidaka, Y.; Nakamura, T.; Tanaka, H.; Inami, K.; Kawano, H. *Int. J. Chem. Kinet*. **1990**, *22*, 701.
(10) Curran, H.; Simmie, J. M.; Dagaut, P.; Voisin, D.; Cathonnet, M. *Proceedings of the 26th Symposium (International) on Combustion*; The Combustion Institute: Pittsburgh, 1996; p 613.
(11) Davis, S. G.; Law, C. K.; Wang, H. *Proceedings of the 27th Symposium (International) on Combustion*; The Combustion Institute: Pittsburgh, 1999; p 305.
(12) Dean, A. M.; Westmoreland, P. R. *Int. J. Chem. Kinet*. **1987**, *19*, 207.
(13) Diau, E. W.; Lin, M. C.; Melius, C. F. *J. Chem. Phys*. **1994**, *101*, 3923.
(14) Alkemade, U.; Homann, K.H. *Z. Physik. Chem. Neue Folge* **1989**, *161*, 19.
(15) Stein, S. E.; Walker, J. A.; Suryan, M. M.; Fahr, A. *Proceedings of the 23rd Symposium (International) on Combustion*; The Combustion Institute: Pittsburgh, 1991; p 85.
(16) Miller, J. A.; Melius, C. F. *Combust. Flame* **1992**, *91*, 21.
(17) Communal, F.; Thomas, S. D.; Westmoreland, P. R. Presented at the 23rd Symposium (International) on Combustion, The Combustion Institute, Pittsburgh, 1991; Poster P40.
(18) Wang, H.; Frenklach, M. *Combust. Flame* **1997**, *110*, 173.
(19) Miller, J. A. Chemical Kinetics and Combustion Modeling. Presented at the 215th National Meeting of the American Chemical Society, Div. Phys. Chem., Dallas, Texas, March 29−April 2, 1998.
(20) For example, see: Hohenberg, P.; Kohn, W. *Phys. Rev. B* **1964**, *136*, 864. Kohn, W.; Sham, L. J. *Phys. Rev. A* **1965**, *140*, 1133. Parr, R. G.; Yang, W. *Density-Functional Theory of Atoms and Molecules*; Oxford University Press: Oxford, 1989.
(21) Curtiss, L. A.; Raghavachari, K.; Trucks, G. W.; Pople, J. A. *J. Chem Phys.* **1991**, *94*, 7221.
(22) Holbrook, K. A.; Pilling, M. J.; Robertson, S. H. *Unimolecular Reactions*, 2nd ed.; Wiley: Chichester, 1996.
(23) Gilbert, R. G.; Smith, S. C. *Theory of Unimolecular and Recombination Reactions*; Blackwell Scientific: Oxford, 1990.
(24) Honjou, N.; Pacansky, J.; Yoshimine, M. *J. Am. Chem. Soc.* **1984**, *106*, 5361; **1985**, *107*, 5332.
(25) Yoshimine, M.; Pacansky, J.; Honjou, N. *J. Am. Chem. Soc.* **1989**, *111*, 2785.
(26) Yoshimine, M.; Pacansky, J.; Honjou, N. *J. Am. Chem. Soc.* **1989**, *111*, 4198.
(27) Walsh, R. J. *J. Chem. Soc., Faraday Trans. 1* **1976**, *72*, 2137.
(28) Karni, M.; Oref, I.; Barzilai-Gilboa, S.; Lifshitz, A. *J. Phys. Chem.* **1988**, *92*, 6924.
(29) Brezinsky, K.; Litzinger, T. A.; Glassman, I. *Int J. Chem. Kinet*. **1984**, *16*, 1053.
(30) Litzinger, T. A.; Brezinsky, K.; Glassman, I. *Combust. Flame* **1986**, *63*, 251.
(31) Frisch, M. J.; Trucks, G. W.; Schlegel, H. B.; Gill, P. M. W.; Johnson, B. G.; Robb, M. A.; Cheeseman, J. R.; Keith, T.; Petersson, G. A.; Montgomery, J. A.; Raghavachari, K.; Al-Laham, M. A.; Zakrzewski, V. G.; Ortiz, J. V.; Foresman, J. B.; Cioslowski, J.; Stefanov, B. B.; Nanayakkara, A.; Challacombe, M.; Peng, C. Y.; Ayala, P. Y.; Chen, W.; Wong, M. W.; Andres, J. L.; Replogle, E. S.; Gomperts, R.; Martin, R. L.; Fox, D. J.; Binkley, J. S.; Defrees, D. J.; Baker, J.; Stewart, J. P.; Head-Gordon, M.; Gonzalez, C.; Pople, J. A. *Gaussian 94*, revision D.4; Gaussian, Inc.: Pittsburgh, PA, 1995.
(32) Stephens, P. J.; Devlin, F. J.; Chablowski, C. F.; Frisch, M. J. *J. Phys. Chem.* **1994**, *98*, 11623.
(33) (a) Becke, A. D. *J. Chem. Phys*. **1992**, *97*, 9173. (b) Becke, A. D. *J. Chem. Phys*. **1993**, *98*, 5648.
(34) Lee, C.; Yang, W.; Parr, R. G. *Phys. Rev.* **1988**, *B37*, 785.
(35) Durant, J. L. *Chem. Phys. Lett*. **1996**, *256*, 595.
(36) Mayer, P. M.; Parkinson, C. J.; Smith, D. M.; Radom, L. *J. Chem. Phys*. **1998**, *108*, 604.
(37) Scott, A. P.; Radom, L. *J. Phys. Chem.* **1996**, *100*, 16502.
(38) Peng, C.; Schlegel, H. B. *Isr. J. Chem.* **1993**, *33*, 449.
(39) Perdew, J. P.; Wang, Y. *Phys. Rev.* **1992**, *B45*, 13244.
(40) Beyer, T.; Swinehart, D. F. *Comm. Assoc. Comput. Machines* **1973**, *16*, 379.
(41) Whitten, G. Z.; Rabinovitch, B. S. *J. Chem. Phys*. **1963**, *38*, 2466. Whitten, G. Z.; Rabinovitch, B. S. *J. Chem. Phys*. **1964**, *41*, 1883.
(42) Astholz, D. C.; Troe, J.; Wieters, W. J. *J. Chem. Phys*. **1979**, *70*, 5107.
(43) (a) Wang, H. Detailed Kinetic Modeling of Soot Particle Formation in Laminar Premixed Hydrocarbon Flames. Ph.D. Thesis, The Pennsylvania State University, University Park, PA, 1992. (b)Wang, H.; Frenklach, M. *J. Phys. Chem.* **1994**, *98*, 11465.
(44) Gilbert, R. G.; Luther, K.; Troe, J. *Ber. Bunsen-Ges. Phys. Chem*. **1983**, *87*, 169.
(45) Kee, R. J.; Rupley, F. M.; Miller, J. A. Sandia Report SAND 89-8009B; Sandia National Laboratories: Albuquerque, NM, 1989.
(46) Lutz, A. E.; Kee, R. J.; Miller, J. A. Sandia Report SAND87-8248; Sandia National Laboratories: Albuquerque, NM, 1988.
(47) Kee, R. J.; Warnatz, J.; Miller, J. A. Sandia Report SAND 83-8209; Sandia National Laboratories: Albuquerque, NM, 1983.
(48) Bailey, I. M.; Walsh, R. J. *J. Chem. Soc., Faraday Trans. 1* **1978**, *74*, 1146.
(49) Bradley, J. N.; West, K. O. *J. Chem. Soc., Faraday Trans. 1* **1975**, *71*, 967.
(50) Kiefer, J. H.; Kumaran, S. S.; Mudipalli, P. S. *Chem. Phys. Lett*. **1994**, *224*, 51.
(51) Tsang, W. In *Heats of Formation of Organic Free Radicals by Kinetic Methods in Energetics of Organic Free Radicals*; Martinho Simoes, J. A., Greenberg, A., Liebman, J. F., Eds.; Blackie Academic and Professional: London, 1996; p 22.
(52) Burcat, A.; McBride, B. *1997 Ideal Gas Thermodynamic Data for Combustion and Air-Pollution Use*; Technion Aerospace Engineering (TAE) Report 804, June 1997.
(53) Whytock, D. A.; Payne, W. A.; Stief, L. J. *J. Chem. Phys*. **1976**, *65*, 191.
(54) Wagner, H. Gg.; Zellner, R. *Ber. Bunsen-Ges. Phys. Chem*. **1972**, *76*, 518.
(55) Aleksandrov, E. N.; Arutyunov, V. S.; Dubrovina, I. V.; Kozlov, S. N. *Kinet. Catal*. **1981**, *21*, 1323.
(56) Wagner, H. Gg.; Zellner, R. *Ber. Bunsen-Ges. Phys. Chem*. **1972**, *76*, 667.
(57) Tsang, W.; Walker, J. A. *J. Chem. Phys*. **1992**, *96*, 8378.
(58) Holt, P. M.; Kerr, J. A. *Int. J. Chem. Kinet.* **1977**, *9*, 185.
(59) Garcia-Dominguez, J. A.; Trotman-Dickenson, A. F. *J. Chem. Soc*. **1962**, 940.
(60) Frenklach, M.; Wang, H.; Bowman, C. T.; Hanson, R. K.; Smith, G. P.; Golden, D. M.; Gardiner, W. C.; Lissianski, V. An Optimized Kinetic Model for Natural Gas Combustion. 25th International Symposium on Combustion, Irvine, California, 1994; Work-In-Progress Poster Session 3, Poster 26.
(61) Kiefer, J. H.; Mizerka, L. J.; Patel, M. R.; Wei, H.-C. *J. Phys. Chem.* **1985**, *89*, 2013.
(62) Miller, J. A.; Volponi, J. V.; Pauwels, J. F. *Combust. Flame* **1996**, *105*, 451.
(63) Kiefer, J. H. *Proceedings of the 27th Symposium (International) on Combustion*; The Combustion Institute: Pittsburgh, 1999; p 113.
(64) Held, T. J. The oxidation of methanol, isobutene and methyl tertiary-butyl ether. Ph.D. Dissertation, Princeton University, Princeton, NJ, 1993.